View metadata, citation and similar papers at core.ac.uk

brought to you by CORE

provided by Enlighten

Schlipf, T.R. and Street, M.W. and Pandavenes, J. and McBride, R. and Cumming, D.R.S. (2003) Design and analysis of a control system for an optical delay-line circuit used as reconfigurable gain equalizer. *Journal of Lightwave Technology* 21(9):pp. 1944-1952.

http://eprints.gla.ac.uk/3875/

Deposited on: 18 January 2008

Glasgow ePrints Service
http://eprints.gla.ac.uk

Design and Analysis of a Control System for an Optical Delay-Line Circuit Used as Reconfigurable Gain Equalizer

T. R. Schlipf, *Member, IEEE*, M. W. Street, J. Pandavenes, R. McBride, and D. R. S. Cumming, *Member, IEEE*

***Abstract*—The design and analysis of a control system for a coherent two-port lattice-form optical delay-line circuit used as reconfigurable gain equalizer is presented. The design of the control system, which is based on a real device model and a least-square optimization method, is described in detail. Analysis on a five-stage device for the 32 possible solutions of phase parameters showed that, for some filter characteristics, the variations in power dissipation can vary up to a factor of 2. Furthermore, the solution selection has influence on the optimization result and number of iterations needed. A sensitivity analysis of the phase parameters showed that the allowable error in the phase parameters should not exceed a standard deviation of $\pi/500$ in order to achieve a total maximal absolute accuracy error not greater than approximately 0.6 dB. A five-stage device has been fabricated using planar lightwave circuit technology that uses the thermooptic effect. Excellent agreement between simulations and measurements has been achieved.**

***Index Terms*—Delay-line circuit, equalizer, gain control, planar lightwave circuit (PLC), thermooptic (TO) effect, tunable optical filter, wavelength-division multiplexing (WDM).**

I. Introduction

OPTICAL telecommunication networks have evolved rapidly since their initial deployment. Early optical networks were point-to-point links containing frequent electrical regenerators to overcome losses in the fiber. The advent of the erbium-doped fiber amplifier (EDFA) replaced the amplification function of electronic regenerators, allowing signals to travel much greater distances while remaining in the optical domain. In addition to the transmission distances of the networks increasing, the capacity of optical networks was also increasing through transmission of higher bit rates.

An additional technique for increasing the capacity is to transmit multiple signals down a single fiber, each carried on different closely spaced optical wavelengths. This technique, known as dense-wavelength-division multiplexing (DWDM) is now a widely deployed transmission scheme. In DWDM systems, EDFAs allow many parallel electrical regenerators to be replaced with individual low-cost amplifiers. Unfortunately, the gain of EDFAs is not uniform across all wavelengths; therefore, in a DWDM system, signals at some wavelengths are amplified more than others. In addition, input power variations, temperature changes, and pump power variations change the power profile of EDFAs. However, it is not only the nonflat spectral responses of EDFAs that lead to a power imbalance in the DWDM channels: reconfiguration, upgrading, and automatic wavelength switching in modern optical networks also cause power variations. In order to minimize system penalties, a device that dynamically compensates for these changes and achieves a flat-gain spectrum is required (Fig. 1). Ideally, this compensation should take part in real time.

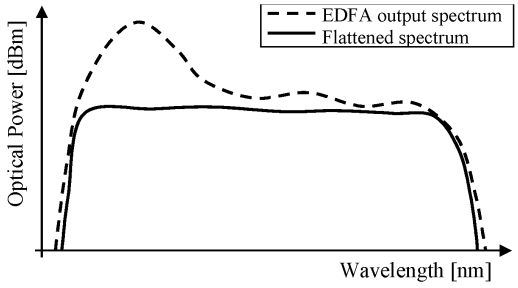

Fig. 1. EDFA output spectrum and flattened spectrum after passing the gain equalizer. *(Reproduced with the permission of Alcatel.)*

A number of different devices have been developed to meet this need [1]–[9]. There are two fundamental approaches: individual channel equalization and Fourier filtering.

Individual channel equalization separates or demultiplexes each channel. For example, individual channel powers can be adjusted with acoustooptic devices and then recombined or multiplexed [2]. However, the use of channel separation and recombination is lossy and prohibitively expensive for large numbers of channels due to the need for multiplexers and multiple optical attenuators.

Dynamic gain equalization through Fourier filtering is based on optical filters typically of third to seventh order (N). The filter coefficients are then dynamically adjusted, independently of the number of channels [3]–[9].

One possible way to realize a Fourier type optical filter is to cascade several stages of variable directional couplers and delay lines with integrated phase shifters, also called an optical delay-line circuit, in planar lightwave circuit (PLC) technology. Reconfigurability and tuning is achieved by building heaters into the waveguides to vary the coupling strength and delay line length via the thermooptic (TO) effect.

Manuscript received February 27, 2003; revised May 21, 2003. The work of T. R. Schlipf is supported in part by the Engineering and Physical Sciences Research Council (EPSRC), U.K., under Award 99317092 and also by Alcatel Optronics Ltd., Livingston, U.K.

T. R. Schlipf is with the Institute for System Level Integration, Livingston EH54 7EG, U.K. (e-mail: thomas.schlipf@sli-institute.ac.uk; thomas.schlipf@alcatel.co.uk).

M. W. Street, J. Pandavenes, and R. McBride are with Alcatel Optronics U.K., Ltd., Livingston EH54 8SF, U.K.

D. R. S. Cumming is with the University of Glasgow, Glasgow G12 8LT, U.K.

Digital Object Identifier 10.1109/JLT.2003.816838

0733-8724/03$17.00 © 2003 IEEE

For such a filter, a synthesis method, which translates the filter coefficients into phase parameters, has been presented by Jinguji *et al.* [10]. They showed that 2^N solutions exist with the same amplitude transfer function but different phase characteristics. Several devices using this principle have been fabricated and their optical performance demonstrated [9]–[11]. However, none of them showed detailed analysis about the selection of the "best" synthesis solution. Furthermore, very little information about the control system required to obtain a reconfigurable or dynamic gain equalizer has been published.

This paper proposes a control system to use the delay-line circuit as a reconfigurable gain equalizer. That is, the operator can configure the device by applying the target filter characteristic. No optical feedback is required. Furthermore, a detailed analysis about the synthesis solutions in terms of power dissipation and accuracy is performed and the allowable phase error of the control parameters is investigated. Finally, a five-stage gain equalizer fabricated in PLC technology is controlled by this concept and the experimental results compared with simulations.

II. Device Concept and Ideal Model

The gain equalizer is a coherent two-port lattice-form optical delay-line circuit [10]. It can be constructed by cascading several stages of a variable directional coupler and a delay line with a phase-shifting element. A schematic of the circuit is shown in Fig. 2.

The number of delay-line stages determines the order N of the filter. Each of the delay stages has the same path-length difference, which sets the free spectral range (FSR) of the filter. Tuning is achieved by changing the variable coupler value and phase-shifting element using the TO effect.

In the domain of digital signal processing (DSP), the delay of the signal introduced by the longer path $\Delta\tau$ is called the unit delay. As shown in Fig. 3, the transfer function of the delay-line circuit agrees with those of finite-impulse response (FIR) digital filters with complex expansion coefficients.

From this, it follows that the filter characteristic of the gain equalizer can be controlled by selecting appropriate complex expansion coefficients. In the DSP domain, many FIR filter design techniques are already developed that extract the FIR parameters from a desired frequency response [12]. Once the complex expansion coefficients are found, the phase parameters are extracted for the directional couplers and the phase-shifting elements in the delay line. The synthesis method [10] used for this purpose is based on the ideal device model shown in Fig. 4.

In this model, the optical delay-line circuit is constructed of several stages. Each stage is composed of the following three basic elements.

- A delay line with a delay time difference of $\Delta\tau$, whose transfer matrix is expressed as

$$S_d = \begin{bmatrix} e^{-j(\omega\Delta\tau/2)} & 0 \\ 0 & e^{j(\omega\Delta\tau/2)} \end{bmatrix} = \begin{bmatrix} z^{-1/2} & 0 \\ 0 & z^{1/2} \end{bmatrix}. \quad (1)$$

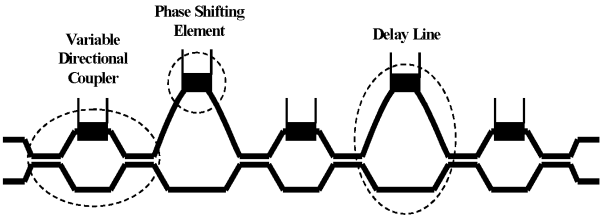

Fig. 2. Two-stage filter consisting of three variable directional couplers and two delay lines with integrated phase-shifting elements. *(Reproduced with the permission of Alcatel.)*

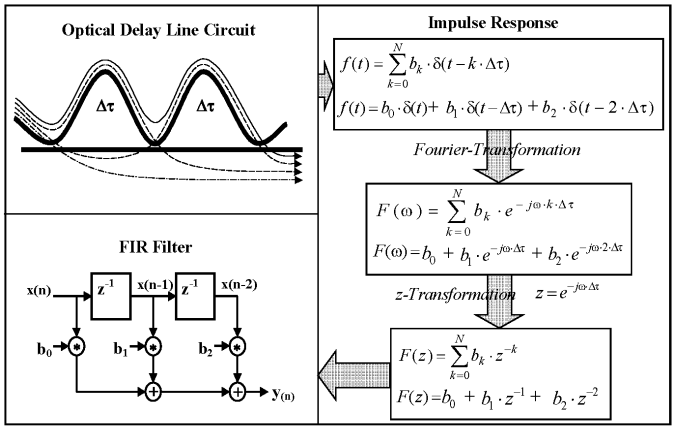

Fig. 3. Transfer function of the optical delay-line circuit is the same as those of a digital FIR filter. *(Reproduced with the permission of Alcatel.)*

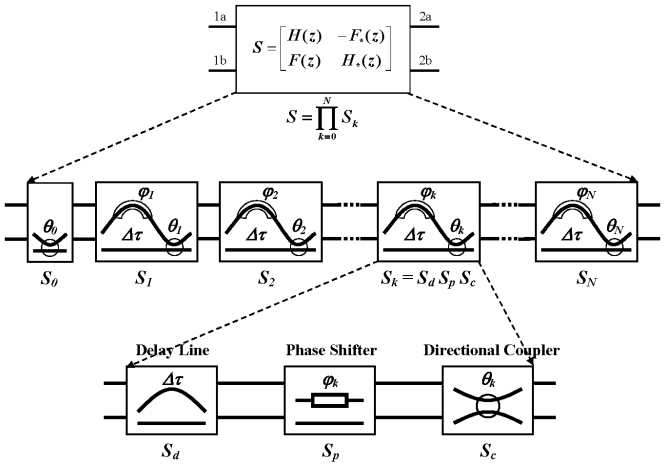

Fig. 4. Ideal device model on which the synthesis method is based on. *(Reproduced with the permission of Alcatel.)*

- A phase-shifting element with a phase-shift value of φ, whose transfer matrix is expressed as

$$S_p = \begin{bmatrix} e^{-j(\varphi/2)} & 0 \\ 0 & e^{j(\varphi/2)} \end{bmatrix}. \quad (2)$$

- A directional coupler with an amplitude-coupling coefficient of $\sin\theta$, whose transfer matrix is expressed as

$$S_c = \begin{bmatrix} \cos\theta & -j\sin\theta \\ -j\sin\theta & \cos\theta \end{bmatrix}. \quad (3)$$

With the synthesis method 2^N solutions for the phase parameters, φ and θ can be obtained from one desired filter transfer characteristic [10]. All have the same amplitude response but different phase characteristics. However, in reality, the optical delay-line circuit does not behave as an ideal component. Nonideal characteristics (e.g., wavelength dependence and differential transmission loss) and other parameters need to be considered. For this reason, a more detailed model of a physically realizable device is needed.

III. Real Device Model

As shown in Fig. 2, the variable directional couplers may be realized as Mach–Zehnder interferometers (MZI) and, hence, implemented as a cascade of a fixed 3-dB coupler acting as a splitter, a phase shifter, and a second 3-dB coupler acting as combiner. The phase shifter within the variable directional coupler can be seen as a delay line with zero-path-length difference. Therefore, each stage consists of two fixed couplers and two delay lines.

Using a transfer matrix model (TMM), the variable coupler and the delay line can be described as follows.

A. Variable Coupler Matrix

Each variable coupler (VC) can be represented by a matrix of the form

$$\mathrm{VC} = F_s(\lambda) \cdot C(\lambda, P) \cdot F_e(\lambda) \tag{4}$$

where the matrices $F_e(\lambda)$ and $F_s(\lambda)$ represent the wavelength-dependent fixed couplers at the input and output of the VC, respectively. The matrix $C(\lambda, P)$ represents the phase-delay section within the VC, which is dependent on the wavelength λ and the applied heater power P.

The transfer matrix of a fixed coupler can be expressed as:

$$F(\lambda) = \begin{bmatrix} \sqrt{1-\kappa(\lambda)} & -j\sqrt{\kappa(\lambda)} \\ -j\sqrt{\kappa(\lambda)} & \sqrt{1-\kappa(\lambda)} \end{bmatrix} \tag{5}$$

where we take a first-order approximation to the wavelength dependence of coupling ratio $\kappa(\lambda)$

$$\kappa(\lambda) = \kappa_{\mathrm{ref}} - \kappa_\lambda \cdot (\lambda - \lambda_{\mathrm{ref}}) \tag{6}$$

where κ_{ref} is the power cross-coupling coefficient at the reference wavelength λ_{ref}.

The transfer matrix of the phase delay section within the VC can be expressed as

$$C(\lambda, P) = \begin{bmatrix} \sqrt{T_c} \cdot e^{-j(\Delta\Theta(\lambda,P)/2)} & 0 \\ 0 & e^{j(\Delta\Theta(\lambda,P)/2)} \end{bmatrix} \tag{7}$$

where T_c is the differential transmission loss between the two arms and $\Delta\Theta(\lambda, P)$ is the phase difference between the arms of the MZI. Expanding to first order in wavelength gives

$$\Delta\Theta(\lambda, P) = 2\pi \left(\Theta_n(P) \cdot \left(1 - \frac{\lambda - \lambda_{\mathrm{ref}}}{\lambda_{\mathrm{ref}}} \right) + n' \cdot \Delta L_c \cdot \frac{\lambda - \lambda_{\mathrm{ref}}}{\lambda_{\mathrm{ref}}} \right). \tag{8}$$

The second part of the summation represents dispersion where n' is the wavelength-dependent waveguide refractive-index parameter and ΔL_c the length difference between the two arms. $\Theta_n(P)$ is the normalized phase shift caused by the length difference of the two arms and the effect of the electrical power applied to the heater in one of the arms.

For small heater powers, Θ_n depends linearly on power dissipation. For larger heater powers, we have found that phase change depends quadratically on the applied power; hence

$$\Theta_n(P) = A_0 + A_1 \cdot P + A_2 \cdot P^2 \tag{9}$$

where A_0 is the phase shift at $P = 0$ introduced by the length difference between the two arms. A_1 and A_2 may be obtained as fitting parameters as part of device characterization.

B. Delay-Line Matrix

Each delay line may be presented by a transfer matrix $D(\lambda, P)$ of the form

$$D(\lambda, P) = \begin{bmatrix} \sqrt{T_d} \cdot e^{-j(\Delta\Phi(\lambda,P)/2)} & 0 \\ 0 & e^{j(\Delta\Phi(\lambda,P)/2)} \end{bmatrix} \tag{10}$$

where T_d is the differential transmission loss between the two arms and $\Delta\Phi(\lambda, P)$ is given by an expression similar to that of (8) for $\Delta\Theta(\lambda, P)$

$$\Delta\Phi(\lambda, P) = 2\pi \left((\Phi_{\mathrm{int}} + \Phi_n(P)) \cdot \left(1 - \frac{\lambda - \lambda_{\mathrm{ref}}}{\lambda_{\mathrm{ref}}} \right) + n' \cdot \Delta L_d \cdot \frac{\lambda - \lambda_{\mathrm{ref}}}{\lambda_{\mathrm{ref}}} \right) \tag{11}$$

where ΔL_d is the length difference between the two arms of the delay line. Φ_{int} is the integer floor part of the phase shift introduced by the length difference between the two arms, and Φ_n is the modulo 2π part of the phase shift caused by the length difference plus the phase shift introduced by heating one of the arms. Φ_n can be expressed as

$$\Phi_n(P) = B_0 + B_1 \cdot P + B_2 \cdot P^2 \tag{12}$$

where B_0 is the modulo 2π part of the phase shift at $P = 0$. B_1 and B_2 may be obtained as fitting parameters as part of device characterization.

IV. The Design Flow

Given the real device model for a gain equalizer, a filter may be synthesized to approximate a given transmission spectrum by calculating in turn: 1) the ideal-device phase coefficients θ and φ; 2) the real-device phase parameters Θ_n and Φ_n; and 3) the required heater power P.

Fig. 5 displays the block diagram of the complete design flow of the control system as used in a reconfigurable gain equalizer.

We implemented this in several steps, as follows.

A. Step 1

In the first step, the complex expansion coefficients b_k ($k = 0 \ldots N$) of the FIR filter are extracted. As already mentioned, this can be done by using various functional approximation methods developed for FIR digital filters. In this

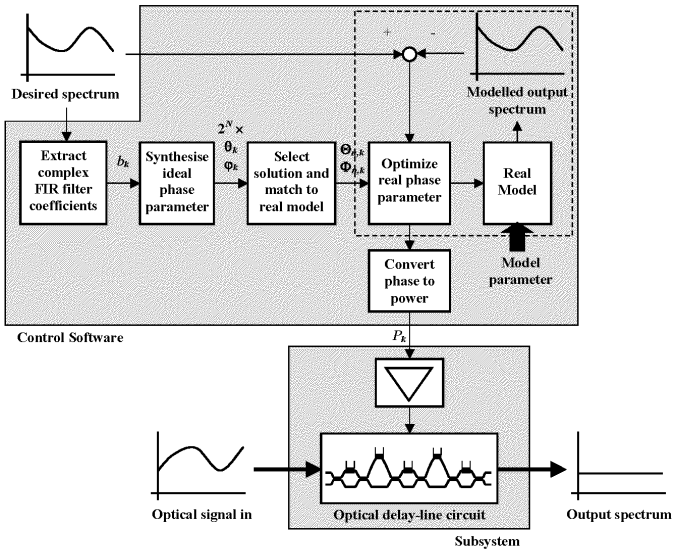

Fig. 5. Complete design flow of the control system as used in a reconfigurable gain equalizer. *(Reproduced with the permission of Alcatel.)*

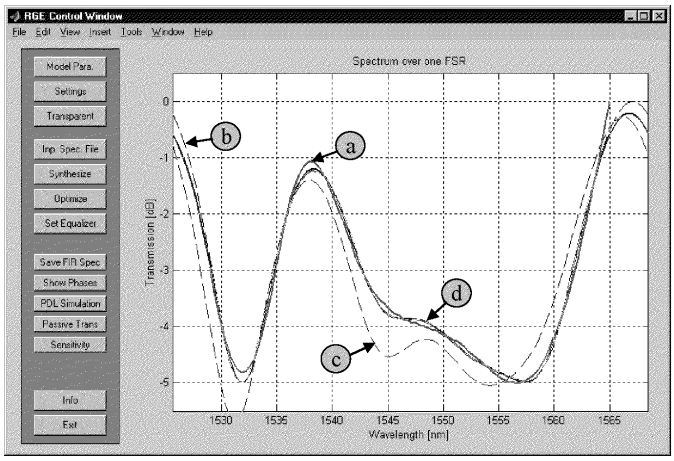

Fig. 6. GUI of control and analysis program in MATLAB. The curves display: (a) target spectrum (inverse EDFA, specified passband 1529 to 1565 nm); (b) best match of an ideal fifth-order FIR filter with optimized complex expansion coefficients; (c) real model response with synthesized phase coefficients prior optimization; and (d) real model response with optimized phase coefficients. *(Reproduced with the permission of Alcatel.)*

application, the frequency sampling method [12] is chosen for the following reasons.

1) It does not follow any standard low-pass, high-pass or bandpass filter response.
2) It consists of complex expansion coefficients.
3) It is characterized by a number of attenuation values across the FSR.

In the frequency sampling method, M samples of the desired frequency response $F_0(z)$ at intervals of kF_s/M $(k = 0 \dots M)$ are obtained from the target wavelength spectrum samples. The filter coefficients $h(n)$ can then be obtained as the inverse Fourier transformation (IFT) of the frequency samples

$$h(n) = \frac{1}{M} \sum_{s=0}^{M-1} H(k) e^{j(2\pi/M)nk} \tag{13}$$

where $H(k)$ $(k = 0 \dots M-1)$ are samples of the ideal or target frequency response $F_0(z)$ over the FSR.

The number of samples M across the FSR is expected to be larger than the order N of the optical delay-line circuit. When the IFT is applied to the M frequency samples, the result is M expansion coefficients. The first $N+1$ coefficients are then used as starting values for a nonlinear least-square curve-fitting algorithm to optimize the expansion coefficients to best fit the FIR filter response to the desired filter characteristic. This optimization procedure is necessary to achieve a good match for the transmission coefficient (in decibels) due to the fact that the desired filter characteristic is only specified in the passband, rather the whole FSR. That is, prior to applying the IFT, the samples outside the specified passband must be extrapolated in order to improve the accuracy in the passband.

After optimization, all expansion coefficients b_k $(k = 0 \dots N)$ of the amplitude transfer function $F(z)$ are obtained.

B. Step 2

In the second step, the ideal phase parameters for the variable directional coupler θ_k $(k = 0 \dots N)$ and for the phase-shifting element in the delay line φ_k $(k = 1 \dots N)$ are calculated following the synthesis method described in [10]. The synthesis method generates N pairs of complex zeros of the polynomial $1 - F(z) \cdot F_*(z)$. Any set of N zeros, one taken from each pair, is a valid solution; hence, there are 2^N solutions. The solutions may be ordered and, hence, identified by sorting in descending order of magnitude of these zeros.

C. Step 3

For an ideal device, any one of these solutions could be used without any difference in the amplitude response of the device. However, the response of the real device shows differences for different sets of these ideal solutions. In addition, some solutions result in lower power consumption in the heaters than others. Therefore, a criterion that defines the "best" solution can be introduced. The following list describes three possible criteria.

- Best approximation to desired spectrum
  Take the solution, which shows the best approximation to the desired spectrum. Possible criterion might be the least-square error in decibels or maximal deviation.
- Least power consumption
  Take the solution with the minimum sum of the phase parameters, hence, the lowest power consumption. As we will show in Section V, different solutions for a five-stage device can yield solutions with variations in power consumption up to a factor of 2.
- Best PDL performance
  Take the solution that results in the lowest PDL. For this criterion, a model that predicts the PDL performance for different sets of phase parameters is necessary.

Once this is completed, the real model phase parameters for the variable directional coupler $\Theta_{n,k}$ $(k = 0 \dots N)$ and for the phase-shifting element in the delay line $\Phi_{n,k}$ $(k = 1 \dots N)$ are

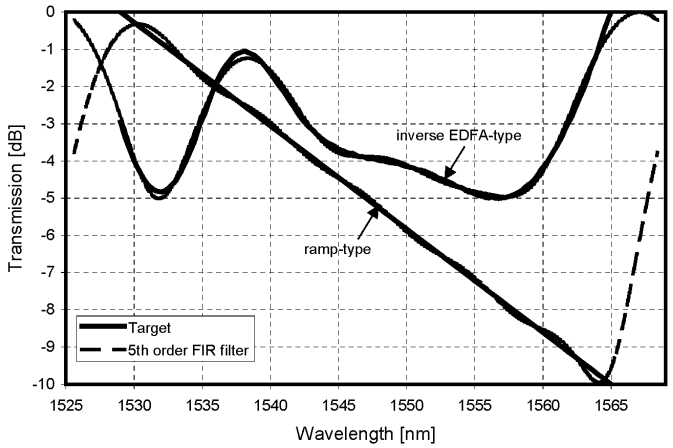

Fig. 7. Inverse EDFA-type spectrum and ramp-type spectrum used for performance evaluation (bold lines). The dashed lines show the best fit of a fifth-order FIR filter with complex expansion coefficients. *(Reproduced with the permission of Alcatel.)*

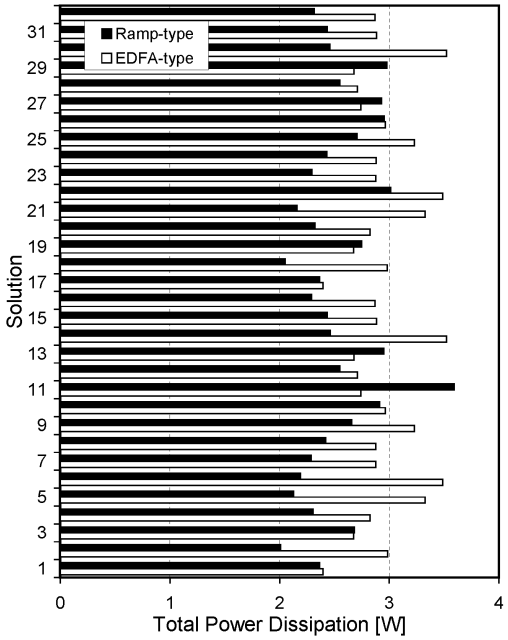

Fig. 8. Power consumption for all 32 possible solutions in a five-stage device extracted for the two spectra shown in Fig. 7. *(Reproduced with the permission of Alcatel.)*

TABLE I
STATISTICAL DATA OF POWER CONSUMPTION SIMULATION

	EDFA	Ramp	Units
Average power consumption	2.94	2.53	W
Standard deviation	0.30	0.34	W
Minimal power consumption	2.40	2.01	W
Maximal power consumption	3.52	3.59	W

derived from the ideal model coefficients θ_k and φ_k. This is needed since the phase parameter description for the variable coupler in the ideal model is different from the description in the real model.

D. Step 4

The calculated phase parameters $\Theta_{n,k}$ and $\Phi_{n,k}$ are then used as starting values for a least-squares optimization using the real device model. This results in phase parameters that "best fit" the real device model response to the desired spectrum. Common algorithms to solve this problem are the Gauss–Newton and the Levenberg–Marquardt method [13]. Simulations showed that the Levenberg–Marquardt method provides the more accurate and more stable results.

E. Step 5

In the final step, the optimized phase parameters for the variable directional couplers $\Theta_{n,k}$ and for the phase-shifting element in the delay lines $\Phi_{n,k}$ are converted into heater powers using (9) and (12), respectively. These electrical power values are then applied to the heating elements via appropriate driving circuitry.

V. SIMULATION RESULTS

Fig. 6 shows the graphical user interface (GUI) of the control and analysis program that we have developed. It shows an inverse EDFA spectrum using the model data of the five-stage device, described hereafter, that was fabricated as an example. The FSR is about 43 nm by design and the center wavelength is chosen to be 1547 nm to cover the whole C band.

Using the above design and analysis tool, several possible simulations have been carried out that are summarized in the following subsections. The real model parameters are taken from the five-stage device fabricated and characterized within Alcatel Optronics.

During the optimization stage, it was found that the number of iterations needed depends on many factors, such as number of points used, target spectrum, and the synthesis solution. However, after less than ten iterations, a satisfactory result could be achieved in almost all cases. Using 50 points along the passband, the time needed for ten iterations on an Intel Pentium 3 processor was approximately 11 s.

A. Power Consumption for Different Solutions

In this simulation, the influence of the selected solution on power consumption for two different target spectra is studied. The chosen target spectra are shown in Fig. 7 and represent an inverse EDFA-type characteristic and a ramp-type characteristic, which might be used for slope compensation. The response of the optimized ideal five-stage FIR filter with complex expansion coefficients is also displayed in Fig. 7.

For each of the target spectra, the design flow is followed as described in Section IV. However, instead of selecting only one solution, all 32 possible solutions were optimized using the real model and converted to heater power values. Fig. 8 shows the resulting total power consumption for all 32 possible solutions.

It can be clearly seen that the choice of the solution has a major influence on the power demand. We have found that for some filter specifications, one solution can dissipate up to twice the power of another. A summary of some statistical values for the two target spectra shown in Fig. 7 can be found in Table I.

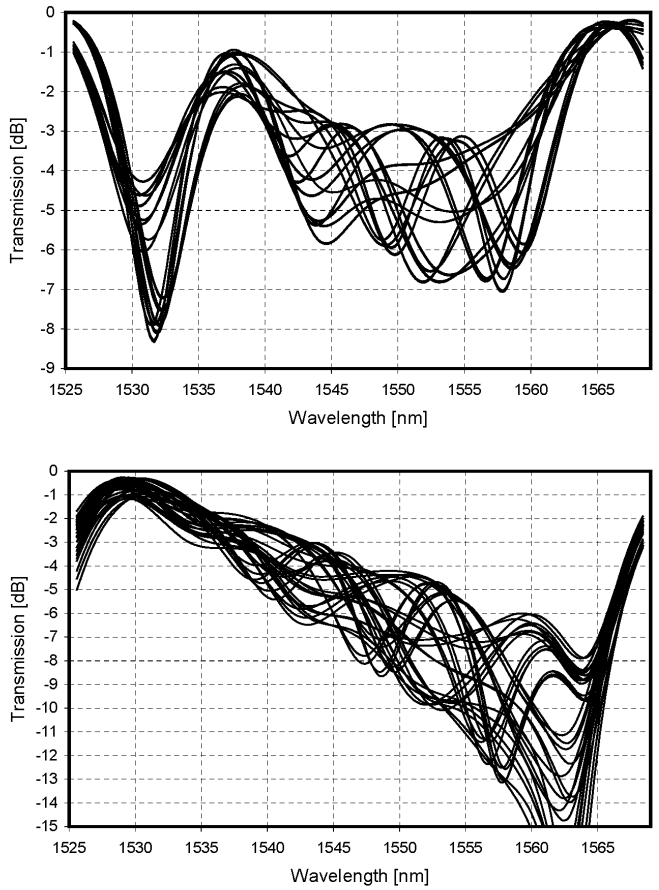

Fig. 9. Real model response using all 32 solution of synthesized and matched-phase parameters prior to optimization for the EDFA-type and ramp-type spectrum shown in Fig. 7. *(Reproduced with the permission of Alcatel.)*

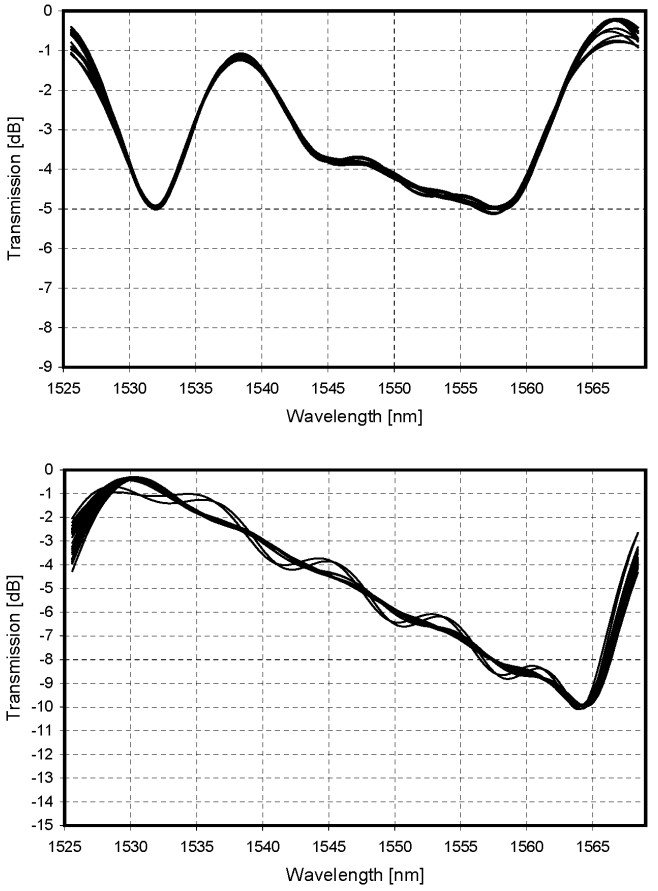

Fig. 10. Real model responses using all 32 solution of optimized phase parameters for the EDFA-type and ramp-type spectrum shown in Fig. 7. *(Reproduced with the permission of Alcatel.)*

In our study we observed that the lowest-power solution for one specification is not necessarily the lowest-power solution for another target spectrum, when solutions are ordered as described in Step 2.

Power consumption for a restricted range of spectra could be reduced by designing the device with specific values of A_0 and B_0 in (9) and (12), respectively. Alternatively, maximum power consumption for an arbitrary spectrum could be roughly halved by differential operation, with additional heating elements supplied at the lower arms of the delay-line circuit. This results in half the phase range needed per heater. However, this also increases the complexity of characterizing the device.

B. Accuracy Prior to and After Optimization for Different Solutions

In this simulation, the accuracy of the real model response is compared with the target filter characteristic. Again, all 32 solutions are used and the phase parameters matched to the real model representation. The model response prior to optimization is shown in Fig. 9 for the same two-target spectra as in the previous simulation (Fig. 7).

It should be noted that for the ideal model, all 32 solutions result in the same amplitude response. This clearly shows that the circuit is very sensitive to nonideal behaviors and that a detailed real model with accurate model parameters is needed in order to optimize the phase parameters further and obtain an

TABLE II
STATISTICAL DATA OF MEAN ABSOLUTE ACCURACY ERROR (MAE) FOR ALL 32 SOLUTIONS

	EDFA	Ramp	Units
Before optimization			
Compared to target spectrum			
Average of MAE	0.902	1.315	dB
Standard deviation of MAE	0.177	0.470	dB
Minimal MAE	0.481	0.726	dB
Maximal MAE	1.172	2.395	dB
Compared to ideal 5th order FIR filter response			
Average of MAE	0.895	1.312	dB
Standard deviation of MAE	0.181	0.468	dB
Minimal MAE	0.453	0.734	dB
Maximal MAE	1.157	2.400	dB
After optimization			
Compared to target spectrum			
Average of MAE	0.108	0.117	dB
Standard deviation of MAE	0.016	0.082	dB
Minimal MAE	0.092	0.070	dB
Maximal MAE	0.144	0.425	dB
Compared to ideal 5th order FIR filter response			
Average of MAE	0.046	0.054	dB
Standard deviation of MAE	0.035	0.095	dB
Minimal MAE	0.008	0.006	dB
Maximal MAE	0.110	0.402	dB

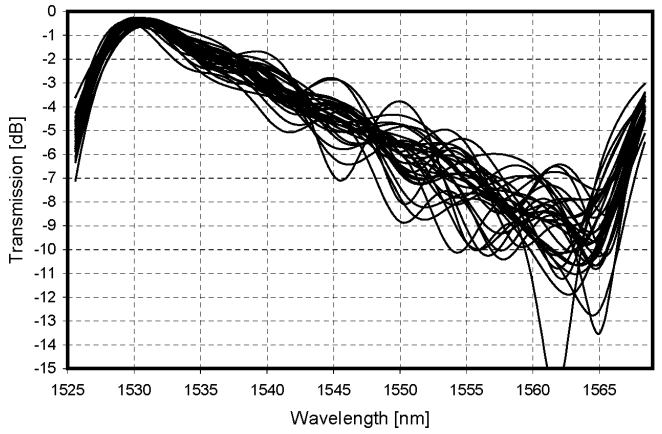

Fig. 11. Sensitivity analysis for a ramp-type filter response with random phase variations with a standard deviation of $\pi/50$. *(Reproduced with the permission of Alcatel.)*

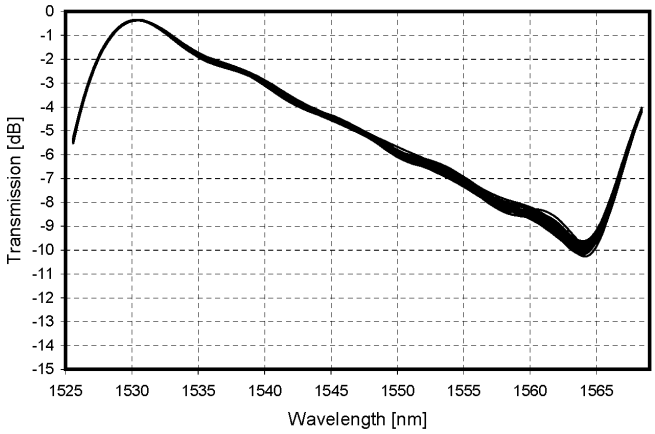

Fig. 12. Sensitivity analysis for a ramp-type filter response with random phase variations with a standard deviation of $\pi/500$. *(Reproduced with the permission of Alcatel.)*

improved accuracy. In addition, Fig. 9 makes clear that each solution results in a different filter characteristic. Some solutions are relatively close to the target spectrum, whereas other solutions show big differences. Furthermore, the shape of the target spectrum also has an influence on the "best" solution in terms of accuracy. Where one solution is the best choice for a particular target spectrum, another filter characteristic may favor a different solution.

In the next step, the phase parameters are optimized so that the real model response is the best fit to the target spectrum, expressed in decibels, using the least-square method. The real model responses after optimization are shown in Fig. 10.

After optimization of the various solutions, the real model responses show a good match to the target spectra. Note that the filter consists of five stages only and, hence, cannot take any arbitrary shape—it is limited to a fifth-order Fourier-type characteristic.

There are differences between the various optimized solutions. That is, some of the solutions have better initial values than others, which result in a better model response after optimization. They also need fewer iterations to achieve improved accuracy. Furthermore, it can be seen that some solutions did not converge well. There is no general rule as to which solution to choose—this depends on the target spectrum and the model parameters.

Table II compares the modeled accuracy before and after optimization to the target spectra and the theoretically possible spectra using an ideal fifth-order FIR filter with complex expansion coefficients. Comparing the accuracy achieved to a FIR filter response, rather than to the target spectrum, eliminates the error introduced by choosing an unrealizable shape of target spectrum (for example, a step change). The statistical data shown in Table II compare the mean absolute error (MAE) of the data points in the spectra. The average, standard deviation, minimum and maximum value of the MAEs for all solutions is listed.

From this, it follows that the average of the mean absolute accuracy error for the optimized phase parameters is about 0.05 dB, compared with the ideal FIR filter response. In comparison with the nonoptimized values, the accuracy has improved dramatically.

TABLE III
STATISTICAL DATA OF MEAN ABSOLUTE ACCURACY ERROR (MAE) FOR 32 RANDOM COMBINATIONS AND THE TOTAL MAXIMAL ABSOLUTE ERROR FOR 1000 SAMPLES

	$\sigma = \pi/50$	$\sigma = \pi/500$	Units
Average of MAE	0.582	0.063	dB
Standard deviation of MAE	0.207	0.020	dB
Minimal MAE	0.242	0.031	dB
Maximal MAE	1.119	0.104	dB
Total maximal abs. error *)	7.60	0.56	dB

*) *for 1000 samples*

C. Sensitivity Analysis of Phase Parameters $\Theta_{n,k}$ and $\Phi_{n,k}$

In the sensitivity analysis, the influence of phase parameter variation from their optimized value was investigated. The target vector chosen for this simulation was the ramp-type spectrum shown in Fig. 7, allowing an easier visual evaluation. Only the first of the 32 synthesis solutions was selected (i.e., that with the zeros of highest magnitude, as described in step 2) and the phase parameter optimized to the ramp-type target spectrum.

Once the 11 optimized real phase parameters for the variable directional couplers $\Theta_{n,k}$ ($k = 0 \ldots 5$) and for the phase-shifting element in the delay lines $\Phi_{n,k}$ ($k = 1 \ldots 5$) are obtained, they are randomly modified within a certain limit, and the real model response is calculated. This is done for 32 random combinations with two different limits. In the first simulation run (Fig. 11), the phase parameters $\Theta_{n,k}$ and $\Phi_{n,k}$ are randomly modified based on a normal distribution with a standard deviation σ of 0.01, whereas in the second simulation run (Fig. 12), σ is only 0.001. Note that the phase parameters are fractions of 2π.

In Fig. 11, it can clearly be seen that a variation in the phase parameters of $\pi/50$ introduces large errors. The total maximal absolute error can be as large as 8 dB at a particular wavelength. Errors are typically highest at larger attenuation values. It therefore follows that a higher accuracy in phase parameter is needed for devices with larger dynamic ranges.

The accuracy error of the 32 randomly chosen combinations is summarized in Table III, together with the total maximal absolute error for 1000 combinations.

From this simulation, it follows that for the ramp-type target spectrum, the allowable error in the phase parameters should not exceed a standard deviation of $\pi/500$ in order to achieve a total maximal absolute accuracy error not greater than approximately 0.6 dB.

VI. Device Fabrication and Measurements

A five-stage delay line circuit has been fabricated in silica-on-silicon PLC technology with a 0.7% refractive- index difference between waveguide and cladding. It consisted of five delay lines with a designed path-length difference of 38.62 μm and six variable directional couplers, which have been realized as MZI. The metal film heating elements used had an electrical resistance of approximately 400 Ω and the power needed for a π phase shift was about 212 mW per heater. The size of the die, including all five stages, was 80 $\times$ 25 mm.

For performance measurements, the die has been packaged and integrated into a subsystem (Fig. 13), which included high-precision drive electronics and a thermoelectric temperature controller (TEC).

For this device, the fixed parameters in the real model were measured following a characterization procedure similar to the one described in [9].

The normalized transmissions of the measured device are displayed in Fig. 14, together with the target spectra and the optimized real model responses. The two target spectra chosen have an inverse EDFA-type and a ramp-type characteristic. Note that the EDFA-type spectrum is different from the one used for the aforementioned simulations.

The MAE between the theoretically calculated filter response and the actual measured was 0.29 dB for the EDFA-type spectrum and 0.34 dB for the ramp-type spectrum. Furthermore, Fig. 14 shows that the EDFA-type target spectrum could be equalized with a remaining ripple with a maximal value of 0.56 dB.

In the ramp-type spectrum, it can be seen that the accuracy at higher attenuation levels is relatively poor. This was predicted in the sensitivity analysis, where it was shown that small variations in the phase parameters can cause large errors.

Table IV summarizes the measured accuracy performance.

In general, the theoretically calculated responses using the real model match well with the measured data. Accuracy could be further improved by refining the characterization procedure, giving better model parameters and hence an improved accuracy performance.

Other device performance parameters were also measured, with worst case values across the passband as follows. The insertion loss (IL) of the packaged device was 6.5 dB. The PDL is dependent on the target filter characteristic and was 0.4 dB for the inverse EDFA-type spectrum and 0.8 dB for the ramp-type spectrum. The chromatic dispersion was 0.2 ps/nm and polarization-mode dispersion (PMD) measurements gave a differential group delay of 0.13 ps.

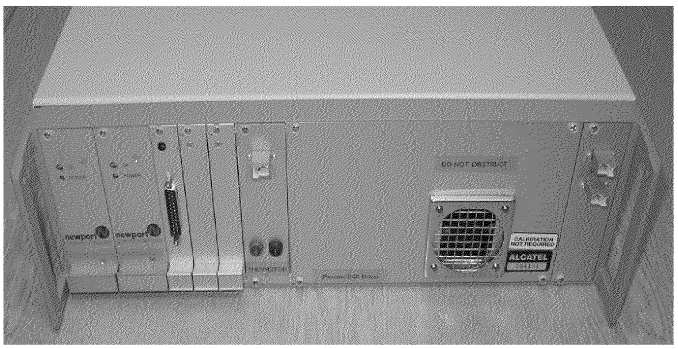

Fig. 13. Photograph of subsystem, including drive electronics and TEC. *(Reproduced with the permission of Alcatel.)*

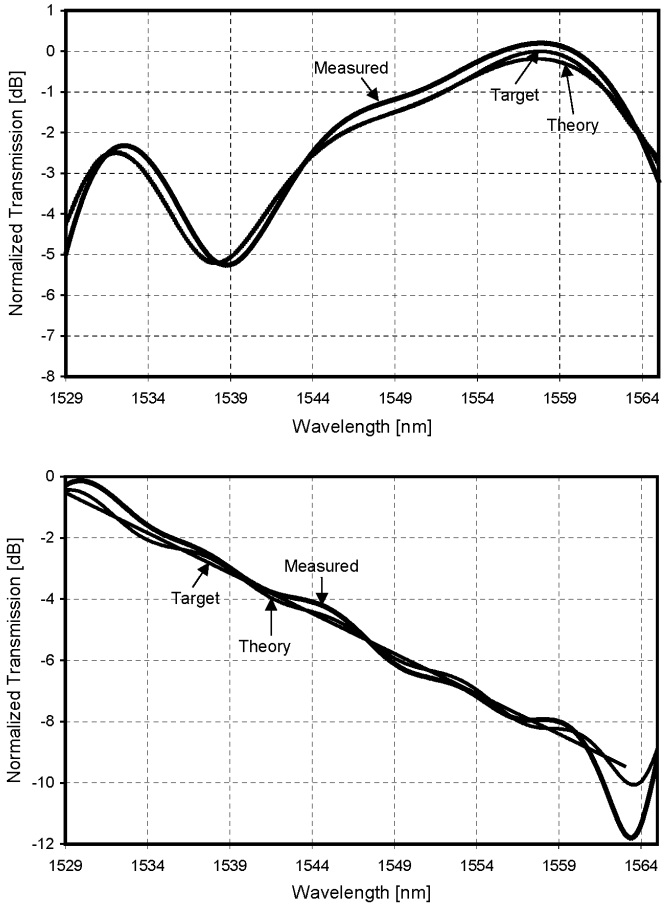

Fig. 14. Measured normalized response of fabricated five-stage device for a inverse EDFA-type and ramp-type filter characteristic. *(Reproduced with the permission of Alcatel.)*

TABLE IV
Measured Accuracy Performance of Fabricated Five-Stage Gain Equalizer in Comparison to Target Spectrum and to Optimized Real Model Response

	EDFA	Ramp	Units
Compared to target spectrum			
Mean absolute error	0.26	0.38	dB
Maximal absolute error	0.56	2.26	dB
Compared to optimized real model response			
Mean absolute error	0.29	0.34	dB
Maximal absolute error	0.71	1.75	dB

VII. Conclusion

We have simulated, developed, and demonstrated a reconfigurable gain equalizer based on a coherent two-port lattice-form optical delay-line circuit with an open-loop control algorithm. The control system generates a set of heater drive powers that best recreate the required filter spectrum. This calculation is based on a one-off characterization of the device—no optical feedback is required.

Our simulations show that the selection of the synthesis solution has a large influence on filter accuracy, on power dissipation, and on the computation time for solution optimization. A factor of two in total power consumption for different solutions has been observed. The selection of the "best" solution depends on the target spectrum, model parameters, and optimization criteria, and no general rule has been identified for selecting an overall ideal solution. A sensitivity analysis on the phase parameters demonstrated that the error should not exceed a standard deviation of $\pi/500$ in order to limit the total accuracy error below approximately 0.6 dB.

Measurements from the five-stage device, fabricated in PLC technology, agreed well with the simulated data. The measured maximal accuracy error of an inverse EDFA-type spectrum was 0.56 dB. This accuracy can further be improved by refining the characterization procedure and the real device model.

References

[1] Y. P. Li and C. H. Henry, "Silica-based optical integrated circuits," *Instit. Elect. Eng. Proc.-Optoelectron.*, vol. 143, no. 5, pp. 263–280, Oct. 1996.

[2] K. M. Feng, J. X. Cai, X. P. Chen, A. E. Willner, and D. A. Smith, "Experimental demonstration of dynamic high-speed equalization of three channels using wavelength demultiplexer and acoustooptic modulators," in *Conf. on Optical Fiber Communication OFC 97*, 1997, pp. 334–335.

[3] P. M. J. Schiffer, C. R. Doerr, W. Stulz, M. A. Capuzzo, E. J. Laskowski, A. Paunescu, and L. T. Gomez, "Smart dynamic wavelength equalizer with on-chip spectrum analyzer," *IEEE Photon. Technol. Lett.*, vol. 12, pp. 1019–1197, Aug. 2000.

[4] J. Chiao and T. Huang, "Liquid-crystal optical harmonic equalizers," in *Proc. Eur. Conf. Optical Communication (ECOC '01)*, vol. 3, 2001, pp. 434–435.

[5] J. E. Ford and J. A. Walker, "Dynamic spectral power equalization using micro-mechanics," *IEEE Photon. Technol. Lett.*, vol. 10, pp. 1440–1442, Oct. 1998.

[6] S. H. Yun, B. W. Lee, H. K. Kim, and B. Y. Kim, "Dynamic erbium-doped fiber amplifier based on active gain flattening with fiber acoustooptic tunable filters," *IEEE Photon. Technol. Lett.*, vol. 11, pp. 1229–1231, Oct. 1999.

[7] T. Saida, K. Okamoto, K. Takiguchi, and T. Shibata, "Dynamic gain equalization filter based on integrated optical transversal filter with asymmetric combiner," *IEE Electron. Lett.*, vol. 38, no. 12, pp. 560–561, June 2002.

[8] K. Suzuki, T. Kitoh, S. Suzuki, Y. Inoue, Y. Hibino, T. Shibata, A. Mori, and M. Shimizu, "PLC-based dynamic gain equalizer consisting of integrated Mach-Zehnder interofermeters with C- and L-band equalizing range," *IEE Electron. Lett.*, vol. 38, no. 18, pp. 1030–1031, August 2002.

[9] B. J. Offrein, F. Horst, G. L. Bona, R. Germann, H. W. M. Salemink, and R. Beyeler, "Adaptive gain equalizer in high-index-contrast SiON technology," *IEEE Photon. Technol. Lett.*, vol. 12, pp. 504–506, May 2000.

[10] K. Jinguji and M. Kawachi, "Synthesis of coherent two-port lattice-form optical delay-line circuit," *J. Lightwave Technol.*, vol. 13, pp. 73–82, Jan. 1995.

[11] C. K. Madsen and J. H. Zhao, *Optical Filter Design and Analysis – A Signal Processing Approach*. New York: Wiley, 1999, pp. 165–236.

[12] E. C. Ifeachor and B. W. Jervis, *Digital Signal Processing – A Practical Approach*. Reading, MA: Addison-Wesley Ltd., pp. 278–373.

[13] *User's Guide of the Optimization Toolbox*, 2 ed., The MathWorks, 2001, pp. 3-18–3-24.

T. R. Schlipf (M'00) received the Dipl.-Ing. (FH) degree in electronics and the M.Sc. degree in signal processing and control from the Fachhochschule Heilbronn, Germany, in 1998 and 1999, respectively.

In 1999, he joined the Eng.D. program in system-level integration at the Institute for System Level Integration, Livingston, U.K. His current research involves the creation of system models for passive optical components in planar lightwave circuit (PLC) and hybrids technology. This includes the development, simulation, and integration of various control mechanisms. The research projects are mainly performed on the site of his sponsoring company Alcatel Optronics U.K. Ltd., Livingston, U.K.

M. W. Street was born in Belfast, Northern Ireland, on August 7, 1969. He received the M.Eng. degree in electrical and electronic engineering from Imperial College, London, U.K., in 1993 and the Ph.D. degree in nonlinear integrated optics from The University of Glasgow, Glasgow, U.K., in 1997.

From 1997 to 2000, he was a Postdoctoral Research Assistant at the University of Glasgow, where he worked on high-speed mode-locked semiconductor lasers. He is currently a Senior Device Development Engineer with Alcatel Optronics U.K., Ltd., working on hybrid planar lightwave component development.

J. Panavenes, photograph and biography not available at the time publication.

R. McBride, photograph and biography not available at the time publication.

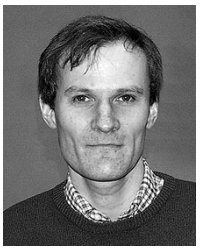

D. R. S. Cumming (M'97) received the B.Eng. degree from University of Glasgow, Glasgow, U.K., in 1989 and the Ph.D. degree from Cambridge University, Cambridge, U.K., in 1993.

He has worked on mesoscopic device physics, radio frequency (RF) characterization of novel devices, fabrication of diffractive optics for optical and submillimeter-wave applications, and microelectronic design. He is presently a Senior Lecturer and EPSRC Advanced Research Fellow in Electronics and Electrical Engineering at the University of Glasgow, where he leads the Microsystem Technology Group.